

Tunable Luminescence From a Single Free-Base Porphyrin Molecule By Controlled Access to Optically Active States

Eve Ammerman ,* Nils Krane , and Bruno Schuler 

nanotech@surfaces Laboratory, Empa – Swiss Federal Laboratories for Materials Science and Technology, Dübendorf 8600, Switzerland

E-mail: eve.ammerman@empa.ch

January 26, 2026

Abstract

Scanning tunneling microscopy-induced luminescence (STML) provides access to optical properties of individual molecules through a cascade of relaxation processes between many-body states. Insufficient charge attachment energies quench the relaxation cascade via optically excited states, causing even intrinsically bright molecules to remain dark in STML. Here, we leverage substrate work function control and tip-induced gating of the double barrier tunnel junction to induce an energy shift of the ionic transition state of a single free-base tetrabenzoporphyrin (H_2TBP) to control access to optically excited states and bright exciton emission. The experimental observations are validated by a rate equation and polaron model considering the relaxation energy of the NaCl decoupling layer upon charging of the molecule.

Introduction

Understanding the optoelectronic (photophysical) properties of organic molecules, such as porphyrins, is technologically relevant for organic light emitting diodes (OLEDs) and organic photovoltaics,¹ and fundamentally important for understanding biological systems, such as photosystem I & II.^{2,3} Recent developments in on-surface synthesis methods have led to the incorporation of porphyrins alongside π -radical magnetic nanographenes,⁴⁻⁷ resulting in tailor-made molecular structures with engineered electronic, magnetic, and optical properties. Porphyrins offer unique opportunities for optical and spin tunability through metalation of the core and coordination chemistry, thereby enabling exciting prospects for engineering the coupling in hybrid porphyrin-nanographene structures.

Scanning tunneling microscopy (STM) provides access to single molecules and orbital resolved electronic measurements. Additionally, STM luminescence (STML) allows probing of their optical properties with characterization comparable to both fluorescence and IR spectroscopy.⁸⁻¹¹ Phthalocyanine (H_2Pc) chromophores, structurally analogous to free-base tetrabenzoporphyrins (H_2TBP), have become the benchmark system in STML studies.^{9,10,12-17} In contrast, nanoscale optical characterization of porphyrins remains surprisingly scarce,¹⁸⁻²² despite their central role in surface science.²³

Although H_2TBP and H_2Pc share a benzene-annulated tetrapyrrolic framework, differences in the macrocycle composition lead to distinct photophysics.²⁴ In H_2Pc , the meso positions are occupied by nitrogen atoms instead of carbon, increasing electronic delocalization and rigidity.²⁵ Consequently, they exhibit different excited-state relaxation dynamics, although both families generally maintain high fluorescence quantum yields.²⁴

Here we show that H_2TBP are inherently dark in single-molecule electroluminescence on Ag(111) due to unfavorable energy alignment. H_2TBP has a smaller hole attachment energy than the chemical analog H_2Pc , suppressing STML emission by $\sim 98\%$ compared to H_2Pc on Ag(111). By locally tuning the electrostatic environment, either via substrate work function or tip-induced gating in a double-barrier tunnel junction, we can overcome this

limitation; accessing otherwise forbidden optical transitions and activating bright emission from individual H₂TBP molecules.

Results and Discussion

Molecular ionic transition state energy on few layer NaCl

STML measurements are performed on individual H₂TBP and H₂Pc molecules decoupled from a Ag(111) substrate by 3 ML insulating NaCl islands, as sketched in Fig. 1. Fig. 1b shows the corresponding STML spectrum of H₂Pc (black) recorded with an excitation rate of 63 pA at -2.5 V and acquisition time of 30 s. The dominant peak 1.81 eV and its lower energy vibronic satellites can be assigned to the S₁ (or Q_x) emission line and the weaker spectral lines around 1.94 eV to the S₂ (or Q_y) emission, in agreement with literature.¹⁴ The STML spectrum on the nearby H₂TBP molecule (orange), taken with the same tip, shows a peak at 1.91 eV, which we assign to S₁, and no emission at higher energy could be detected. Strikingly, the emission intensity of H₂TBP is significantly weaker than the H₂Pc emission, necessitating a higher excitation current (150 pA) and relatively long integration time (120 s). After normalizing the luminescence spectra to photon counts per tunneled electron, the H₂TBP spectrum has 50 times less intensity than the H₂Pc spectrum. Such a low photon yield of H₂TBP poses a significant challenge for experiments requiring high sensitivity, such as high-resolution fluorescence mapping,¹⁰ detection of weak vibronic satellite emission,^{14,26,27} or potential phosphorescence on metalated porphyrins.²⁸

To explain the dark emission of H₂TBP we adopt the many-body description of molecular electronic states introduced by Miwa et al. to explain the STML excitation mechanism²⁹ and later applied by Jiang et al. to construct an extensive description of electronic excitation and optical emission arising from changes to static molecular charge state.³⁰ In the many-body framework, the energy level alignment between a transient charge state and the optically excited state should be considered to be the primary factor restricting fluorescence of H₂TBP

on Ag(111). Scanning tunneling spectroscopy (STS) measurements of H₂TBP and H₂Pc (Fig. 1c) were recorded at the same tip positions as the STML spectra in Fig. 1b. The STS spectra reveal a pronounced upward shift of the positive and negative ion resonances of H₂TBP relative to H₂Pc, accompanied by an increased transport gap. This shift can be attributed to the presence of four additional electronegative nitrogen atoms in the H₂Pc macrocycle.

At first glance, the observed shift does not appear to limit electro-excitation of H₂TBP. The onset of the positive ion resonance (PIR) in the STS spectra appears at an applied bias of -2.1 V suggesting a nominal energy of 2.1 eV of the positively charged molecule (D_0^+) upon hole injection. This energy lies approximately 200 meV above the optical emission line at ~ 1.91 eV, seemingly satisfying the energy requirement for electroluminescence. However, this interpretation neglects the relaxation processes accompanying molecular charging on the surface. In particular, the ionic NaCl surface has been shown to substantially contribute to the reorganization energy and resonance broadening.^{31,32} Using a polaron model, Vasilev et al. demonstrated for H₂Pc on NaCl that the true ground-state energy of the positively charged molecule lies substantially below the ion resonance onsets observed in STS.²⁷ The apparent offset and broadening of the ion resonance in STS arise from structural relaxation of the NaCl environment during hole injection. This relaxation leads to an apparent D_0^+ energy shifted by an amount comparable to the charge-state relaxation energy, λ_+ , as illustrated in Fig. ???. To account for the structural relaxation of the NaCl and the corresponding broadening of the STS spectra in Fig. 1c, we apply a polaron model adapted from Ref. 27. The model is fit to the STS spectra and estimates a D_0^+ energy of 1.81 eV for H₂TBP, after accounting for a voltage drop of 10% , and a D_0^+ energy of 1.98 eV for H₂Pc. The results suggest the D_0^+ energy of H₂Pc is about 200 meV higher than its S_1 state at 1.81 eV, enabling the $D_0^+ \rightarrow S_1$ transition and, accordingly, bright emission from H₂Pc. On the other hand, for H₂TBP, the D_0^+ energy is ~ 100 meV lower than the respective S_1 state and emission should be fully quenched. To explain the experimentally observed STML intensity one needs to

consider the dielectric and geometric properties of the STML tunnel junction.

Tuning the local electrochemical potential

In a double-barrier tunneling junction (DBTJ) geometry, a fraction of the applied bias voltage drops across the insulating film, leading to a shift in the electrochemical potential (ΔE) of the adsorbed molecule with respect to the substrate.³³ For molecules on few-layer (3-4 ML) NaCl, a voltage drop of $\sim 10\%$ can be estimated.²⁷ The STML measurements are typically performed with applied absolute voltages in the range of 2-3 V providing an effective gating voltage of 200-300 meV, which is on the order of the energy difference between the H_2TBP D_0^+ and S_1 states. Hence, this gating effect is expected to lift the D_0^+ state energy across the transition threshold to S_1 leading to an emission intensity strongly dependent on the applied bias.

The voltage dependence can be understood when we examine the relative transition rates between the D_0^+ charge state and the optical state S_1 . Fig. 2a illustrates the many-body state diagram relative to the ground state (S_0). The D_0^+ state energy calculated with the polaron fit on Ag(111) lies about 100 meV below the S_1 state without any bias applied, preventing the transition and subsequent radiative relaxation. With a negative bias voltage applied to the STM junction D_0^+ is shifted upwards by $\Delta E(V)$ due to the voltage drop, enabling access to the $D_0^+ \rightarrow S_1$ transition. This effect can be observed experimentally, by taking STML spectra at different bias voltages and constant tip height. The normalized emission intensities of the S_1 line show a clear increase with bias voltage as displayed in Fig. 2b.

Using a simple rate equation model,³⁴ we simulated the shift in the electrochemical potential (top axis of Fig. 2b) and the resulting voltage dependence of the emission rate (dashed blue line in Fig. 2b), which are in good agreement with the experiment (black dots). The voltage-dependent transition rates for $S_0 \rightarrow D_0^+ \rightarrow S_1$ were derived from the polaron model, using the relaxation energy obtained from a fit to the experimental STS data. Because both the tip height and lateral position strongly influence the local voltage drop and

tunneling rate, these quantities were treated as adjustable parameters in the model. The resulting energy shift, ΔE , scales with a voltage drop of 10.2% which is within the expected range of 10-15%. More details on the model and its implementation are provided in the SI.

Lastly, during our STML measurements two electronic excitations are required to access the optically active states, $S_0 \rightarrow D_0^+ \rightarrow S_1$. Each excitation can be treated as independent charge state transition and both are subject to a resonance shift and broadening due to the underlying NaCl layer. Therefore, despite a shift of $\Delta E > 200$ meV for bias voltages at the onset of the PIR, luminescence remains below the experimental detection limit. It is not sufficient to simply raise the D_0^+ energy above S_1 but a larger shift is needed to compensate for said resonance shift and broadening. Extrapolation of the rate equation model to more negative bias voltages shows, that the emission intensity of H_2TBP on $Ag(111)$ is still quenched by 94% for bias voltages around -2.5 V. The model indicates a bias voltage < -5.6 V, $\Delta E \geq 560$ meV, is needed to achieve optimal energy level alignment. Applying such a large bias voltage in an experiment would lead to unwanted effects, including a transition from the tunneling regime to field emission which would result in a loss of spatial resolution and risk damage to the molecule being studied.

Engineered energy level alignment for optical characterization

For this reason, the chemical potential shift induced by the voltage drop in the STM junction provides only limited tuning range. The local gating effect is insufficient to fully overcome the energetic constraint limiting the $D_0^+ \rightarrow S_1$ transition, as shown by the strong voltage dependence of the emission intensity. To extend this range, we exploit the intrinsic energy level alignment defined by the substrate work function (Φ), which enables a static shift of the molecular ion resonances. To this end, we performed STML measurements of H_2TBP on 4 ML NaCl deposited on $Ag(110)$. This substrate retains the strong plasmonic enhancement of silver while reducing the work function from $\Phi_{Ag111} = 4.5$ eV to $\Phi_{Ag110} = 4.1$.³⁵ Lowering the workfunction by 400 mV is expected to shift the positive ion resonance energies of adsorbed

molecules by a similar amount to higher energies. This shift is confirmed experimentally by comparing the STS spectra of decoupled H₂TBP on Ag(111) and Ag(110), with the PIR on Ag(110) being shifted by 400 meV to -2.5 eV (Fig. 3a). A polaron model fit of the STS spectra on Ag(110) (Fig. ??b) yields a D₀⁺ energy of 2.25 eV, matching the work function shift. The shift in the D₀⁺ state energy provides approximately ~300 meV excess energy relative to the S₁ state, comparable to the D₀⁺ → S₁ transition of H₂Pc on Ag(111). Correspondingly, STML measurements of H₂TBP on Ag(110) reveal a significant increase in the emission intensity by nearly two orders of magnitude and the appearance of an additional emission line at 2.15 eV, tentatively assigned to S₂ (Fig. 3b).

In Fig. 3c, the voltage dependence of the normalized emission intensity is shown. It exhibits a clear plateau as soon as the applied voltage reaches the onset of the PIR (Fig. 3c), in contrast with the observations for H₂TBP on NaCl/Ag(111), where the emission increases gradually, even at voltages significantly beyond the PIR (Fig. 2b). By engineering the level alignment we shift the D₀⁺ sufficiently high in energy that the D₀⁺ → S₁ transition becomes "saturated" and does not increase anymore with more negative bias voltages. Applying the rate-equation model to the STML data reproduces an approximately constant emission rate for S₁. The experimentally observed drop in emission intensity for smaller absolute bias voltages can be explained by a small background current of ~150 fA that skews the normalized intensity to lower values (see Fig. ??). Considering the relatively low amplitude of S₂ compared to S₁ (<10%) the majority of bright transitions in STML comes from S₁, accordingly S₂ was neglected for modeling S₁ emission. The bright emission and nearly constant voltage dependence observed for H₂TBP on Ag(110) coincides with an energy level shift comparable to the relaxation energy and corresponding vibrational broadening of charge state transitions estimated for the NaCl surface.

High-resolution mapping of vibronically-resolved emission in a single H₂TBP

The increased electroluminescence quantum yield allows for intra-molecular fluorescence mapping, revealing vibronic fine-structures previously inaccessible. Hyperspectral optical imaging provides direct insight into the photophysics of the porphyrin, capturing both spatially resolved emission and its vibronic fingerprints.^{11,14,36}

Porphyrin molecules are well known for exhibiting significant Franck-Condon (FC) and Herzberg-Teller (HT) coupling enabling intensity borrowing and non-adiabatic transitions between excited states.³⁷⁻³⁹ High-resolution STML spectra of H₂TBP reveal a series of well-resolved vibronic sidebands that reflect coupling between electronic and vibrational degrees of freedom (Fig. 4a,b). These features can be modeled using time-dependent density functional theory (TD-DFT). Calculated FC spectra, with and without HT contributions to the vibronic emission of the S₁ and S₂ states, are shown in Fig. 4c and Fig. 4d, respectively. For both S₁ and S₂, the simulated FC-HT components of the spectra show good agreement with the experimental STML data. The results clearly indicate that HT contributions play a significant role in reproducing the spectra, as expected for porphyrins.³⁷ The agreement is particularly strong for S₁, where, both, the peak positions and relative intensities are well captured. The simulated spectra were calculated for the far-field without taking into account the orientation of the transition dipole moment; however, STML does provide the spatial resolution to distinguish between FC and HT modes with orthogonal transition dipole moment.²⁷ Comparison of the two spectra taken along different axes of H₂TBP (red and grey in Fig 4a and b) shows the same vibronic fingerprint, indicating fast tautomerization processes and therefore an averaging effect of the two tautomers.¹⁰

Some deviations are, however, observed for S₂, most notably around -175 meV, where theory predicts intense vibronic peaks that appear much weaker experimentally, and near -50 meV, where additional peaks are present in the data but absent in the calculations. These discrepancies may arise from substrate-induced distortions of the molecular geometry,

that are not captured in TD-DFT calculations based on the gas phase geometry. The local electrostatic environment of the NaCl film can be expected to perturb the molecular conformation, affecting the ordering and intensity of vibrational modes.

Having established the vibronic structure of H₂TBP emission, we next examine the spatial distribution of the S₁ and S₂ states using hyper-resolved fluorescence maps. These maps provide direct insight into how the emission intensity varies across the molecule for each excited state. Experimentally, they were obtained by recording hyperspectral STML data on a dense grid and extracting the intensity at the zero-phonon line. The resulting maps for S₁ and S₂ are shown in the top panels of Fig. 4e and Fig. 4f, respectively. The corresponding simulated maps (bottom panels) were generated by convoluting the TD-DFT transition densities of the S₁ and S₂ states with the tip plasmonic potential.^{10,40}

In the simulations, both states exhibit mirror symmetry with clear nodal planes oriented orthogonally to each other. The experimental S₁ map lacks distinct nodal planes and instead exhibit a dual-mirror symmetry that can be explained by tautomerization processes, previously reported for STML of H₂Pc.¹⁰ In contrast, the nodal plane of the simulation can be seen in the experimental S₂ map but is accompanied by a 4-fold symmetry that is not aligned with the symmetry axes of the molecule. The apparent deviation in the S₂ map may contain insights into the dynamics of the tautomerization process and merits further investigation.

Conclusions

In summary, we have shown that tuning the hole-attachment energy via tip-induced gating or by controlling the substrate work function enables efficient electrical excitation and bright excitonic emission from single H₂TBP molecules. Quantitative analysis of the hole attachment energy using a polaron model highlights the critical role of the NaCl decoupling layer relaxation energy in determining the energy requirements for transitions into the optically

excited state. The voltage-dependent STML emission could be modeled by rate equations that consider the NaCl relaxation energy extracted from STS. The bright emission of H₂TBP on NaCl(4ML)/Ag(110) allowed us to perform hyper-resolved fluorescence mapping and to resolve the electronic and vibronic structure of individual excited states. Comparison with TD-DFT calculations reveals that Herzberg–Teller coupling plays a central role in shaping the vibronic emission, while hyperspectral mapping exposes distinct spatial signatures of the S₁ and S₂ states. Together, these results show that we have achieved access to the photophysics of a single free-base porphyrin with exceptional spectral and spatial resolution. STML spectra recorded at the intramolecular level provides a detailed view of the cascade of relaxation processes producing electronic and vibronic fingerprints of distinct excited states. The STML experiments enabled by controlled energy level alignment offer an opportunity to build a comprehensive picture of the photophysics of free-base porphyrins.

Methods

Sample Preparation

Sample preparation of H₂TBP and H₂Pc decoupled from Ag(111) and Ag(110) by thin-films of NaCl. Sputter and anneal of single-crystal silver substrates by repeated argon ion bombardment and heating to 673 K. Growth of NaCl thin-films on Ag surfaces at room temperature by sublimation from a Knudson-type effusion cell at 740 °C and post-annealing to 200 °C for 3-4 ML NaCl on Ag(111) and 230 °C for 4-5 ML NaCl on Ag(110). The difference in NaCl thickness is chosen to achieve comparable topographic heights in STM measurements of ~500-600 pm. In-situ flash-deposition of molecules from a direct-current Si heater with direct line of sight to the STM scan head held at 4.5 K.

STML Measurements of Single Molecules

SPM measurements were performed using a CreaTec Fischer & Co. GmbH scanning probe microscope at liquid helium temperatures ($T < 5$ K) under ultrahigh vacuum ($p < 2 \times 10^{-10}$ mbar). STM and STS measurements performed with a FEMTO-DLPCA200 preamplifier with a gain of 10^9 A/V. Light collection from the STM tunnel junction is done with a silver off-axis parabolic mirror that has a focal length of 33.8 mm and a diameter of 1 inch with an incident angle of 60 degrees and an estimated numerical aperture of 0.4. Optical spectra were collected through a fiber collimator using a Teledyne Princeton Instruments SpectraPro HRS 300 spectrograph, equipped with an LN-cooled PyLoN 400BR eXcelon detector with an estimated spectral resolution of ~ 4 nm and ~ 2 nm after diffracted from a grating of 150 l/mm (Fig. 2b, Fig. 3b/c, Fig. 4a/b) and 600 l/mm (Fig. 1b), respectively. A Ag wire tip was used for all STM and STML measurements and was prepared by repeated indentations into the metallic substrate and voltage pulses. The optical response of the STM tip was optimized by repeated indentation until a plasmonic emission spectra measured on the bare Ag surface at +2.5 V on Ag(111) or -2.5 V on Ag(110) overlapped with the spectral emission of the H₂TBP molecule. Each STML emission spectra is normalized by the tip-specific plasmonic response present at the time of measurement to account for intensity variations of the junction response. For hyper-resolved fluorescence mapping individual STML spectra are recorded at constant tip height on a dense grid with drift correction.

Time-dependent Density Functional Theory

Density functional theory (DFT) and time-dependent DFT (TD-DFT) calculations were performed using B3LYP functional and def2-TZVP basis set within the Gaussian16 software package.⁴¹ TD-DFT used the Tamm-Dancoff approximation (TDA) and the emission spectra were simulated for a Lorentzian lineshape with broadening of 40 cm^{-1} half width at half maximum. All calculations were performed in gas phase.

References

1. Mathew, S.; Yella, A.; Gao, P.; Humphry-Baker, R.; Curchod, B. F. E.; Ashari-Astani, N.; Tavernelli, I.; Rothlisberger, U.; Nazeeruddin, M. K.; Grätzel, M. Dye-sensitized solar cells with 13% efficiency achieved through molecular engineering of porphyrin sensitizers. *Nature Chemistry* **2014**, *6*, 242–247.
2. Jordan, P.; Fromme, P.; Witt, H. T.; Klukas, O.; Saenger, W.; Krauss, N. Three-dimensional structure of cyanobacterial photosystem I at 2.5 Å resolution. *Nature* **2001**, *411*, 909–917.
3. Umena, Y.; Kawakami, K.; Shen, J. R.; Kamiya, N. Crystal structure of oxygen-evolving photosystem II at a resolution of 1.9 Å. *Nature* **2011**, *473*, 55–60.
4. Mateo, L. M.; Sun, Q.; Liu, S.-X.; Bergkamp, J. J.; Eimre, K.; Pignedoli, C. A.; Ruffieux, P.; Decurtins, S.; Bottari, G.; Fasel, R.; Torres, T. On-surface synthesis and characterization of triply fused porphyrin–graphene nanoribbon hybrids. *Angewandte Chemie International Edition* **2020**, *59*, 1334–1339.
5. Sun, Q.; Mateo, L. M.; Robles, R.; Lorente, N.; Ruffieux, P.; Bottari, G.; Torres, T.; Fasel, R. Bottom-up fabrication and atomic-scale characterization of triply linked, laterally pi-extended porphyrin nanotapes. *Angewandte Chemie International Edition* **2021**, *60*, 16208–16214.
6. Chen, Q.; Lodi, A.; Zhang, H.; Gee, A.; Wang, H. I.; Kong, F.; Clarke, M.; Edmondson, M.; Hart, J.; O’Shea, J. N.; Stawski, W.; Baugh, J.; Narita, A.; Saywell, A.; Bonn, M.; Müllen, K.; Bogani, L.; Anderson, H. L. Porphyrin-fused graphene nanoribbons. *Nature Chemistry* **2024**, *16*, 1133–1140.
7. Xiang, F.; Gu, Y.; Kinikar, A.; Bassi, N.; Ortega-Guerrero, A.; Qiu, Z.; Gröning, O.; Ruffieux, P.; Pignedoli, C. A.; Müllen, K.; Fasel, R. Zigzag graphene nanoribbons with periodic porphyrin edge extensions. *Nature Chemistry* **2025**, *17*, 1356–1363.

8. Kuhnke, K.; Große, C.; Merino, P.; Kern, K. Atomic-Scale Imaging and Spectroscopy of Electroluminescence at Molecular Interfaces. *Chemical Reviews* **2017**, *117*, 5174–5222.
9. Doppagne, B.; Chong, M. C.; Bulou, H.; Boeglin, A.; Scheurer, F.; Schull, G. Electrofluorochromism at the single-molecule level. *Science* **2018**, *361*, 251–255.
10. Rosławska, A.; Neuman, T.; Doppagne, B.; Borisov, A. G.; Romeo, M.; Scheurer, F.; Aizpurua, J.; Schull, G. Mapping Lamb, Stark, and Purcell Effects at a Chromophore-Picocavity Junction with Hyper-Resolved Fluorescence Microscopy. *Physical Review X* **2022**, *12*, 011012.
11. Jiang, S.; Neuman, T.; Boeglin, A.; Scheurer, F.; Schull, G. Topologically localized excitons in single graphene nanoribbons. *Science* **2023**, *379*, 1049–1054.
12. Zhang, Y.; Luo, Y.; Zhang, Y.; Yu, Y.-J.; Kuang, Y.-M.; Zhang, L.; Meng, Q.-S.; Luo, Y.; Yang, J.-L.; Dong, Z.-C.; Hou, J. G. Visualizing coherent intermolecular dipole–dipole coupling in real space. *Nature* **2016**, *531*, 623–627.
13. Imada, H.; Miwa, K.; Imai-Imada, M.; Kawahara, S.; Kimura, K.; Kim, Y. Real-space investigation of energy transfer in heterogeneous molecular dimers. *Nature* **2016**, *538*, 364–367.
14. Doppagne, B.; Chong, M. C.; Lorchat, E.; Berciaud, S.; Romeo, M.; Bulou, H.; Boeglin, A.; Scheurer, F.; Schull, G. Vibronic Spectroscopy with Submolecular Resolution from STM-Induced Electroluminescence. *Physical Review Letters* **2017**, *118*, 127401.
15. Zhang, Y.; Meng, Q.-S.; Zhang, L.; Luo, Y.; Yu, Y.-J.; Yang, B.; Zhang, Y.; Esteban, R.; Aizpurua, J.; Luo, Y.; Yang, J.-L.; Dong, Z.-C.; Hou, J. G. Sub-nanometre control of the coherent interaction between a single molecule and a plasmonic nanocavity. *Nature Communications* **2017**, *8*, 15225.

16. Cao, S.; Rosławska, A.; Doppagne, B.; Romeo, M.; Féron, M.; Chérioux, F.; Bulou, H.; Scheurer, F.; Schull, G. Energy funnelling within multichromophore architectures monitored with subnanometre resolution. *Nature Chemistry* **2021**, *13*, 766–770.
17. Doležal, J.; Sagwal, A.; de Campos Ferreira, R. C.; Švec, M. Single-Molecule Time-Resolved Spectroscopy in a Tunable STM Nanocavity. *Nano Letters* **2024**, *24*, 1629–1634.
18. Deng, W.; Fujita, D.; Ohgi, T.; Yokoyama, S.; Kamikado, K.; Mashiko, S. STM-induced photon emission from self-assembled porphyrin molecules on a Cu(100) surface. *The Journal of Chemical Physics* **2002**, *117*, 4995–5000.
19. Liu, H. W.; Nishitani, R.; Han, T. Z.; Ie, Y.; Aso, Y.; Iwasaki, H. STM fluorescence of porphyrin enhanced by a strong plasmonic field and its nanoscale confinement in an STM cavity. *Physical Review B* **2009**, *79*, 125415.
20. Zhu, S.-E.; Kuang, Y.-M.; Geng, F.; Zhu, J.-Z.; Wang, C.-Z.; Yu, Y.-J.; Luo, Y.; Xiao, Y.; Liu, K.-Q.; Meng, Q.-S.; Zhang, L.; Jiang, S.; Zhang, Y.; Wang, G.-W.; Dong, Z.-C.; Hou, J. G. Self-Decoupled Porphyrin with a Tripodal Anchor for Molecular-Scale Electroluminescence. *Journal of the American Chemical Society* **2013**, *135*, 15794–15800.
21. Dong, Z. C.; Zhang, X. L.; Gao, H. Y.; Luo, Y.; Chen, L. G.; Zhang, R.; Tao, X.; Zhang, Y.; Yang, J. L.; Hou, J. G. Generation of molecular hot electroluminescence by resonant nanocavity plasmons. *Nature Photonics* **2010**, *4*, 50–54.
22. Chong, M. C.; Sosa-Vargas, L.; Bulou, H.; Boeglin, A.; Scheurer, F.; Mathevet, F.; Schull, G. Ordinary and Hot Electroluminescence from Single-Molecule Devices: Controlling the Emission Color by Chemical Engineering. *Nano Letters* **2016**, *16*, 6480–6484.
23. Gottfried, J. M. Surface chemistry of porphyrins and phthalocyanines. *Surface Science Reports* **2015**, *70*, 259–379.

24. Lu, H.; Kobayashi, N. Optically Active Porphyrin and Phthalocyanine Systems. *Chemical Reviews* **2016**, *116*, 6184–6261.
25. Stuzhin, P. A.; Khelevina, O. G. Azaporphyrins: structure of the reaction centre and reactions of complex formation. *Coordination Chemistry Reviews* **1996**, *147*, 41–86.
26. Doležal, J.; Canola, S.; Hapala, P.; de Campos Ferreira, R. C.; Merino, P.; Švec, M. Real Space Visualization of Entangled Excitonic States in Charged Molecular Assemblies. *ACS Nano* **2022**, *16*, 1082–1088.
27. Vasilev, K.; Canola, S.; Scheurer, F.; Boeglin, A.; Lotthammer, F.; Chérioux, F.; Neuman, T.; Schull, G. Exploring the Role of Excited States' Degeneracy on Vibronic Coupling with Atomic-Scale Optics. *ACS Nano* **2024**, *18*, 28052–28059.
28. Grewal, A.; Imada, H.; Miwa, K.; Imai-Imada, M.; Kimura, K.; Jaculbia, R.; Kuhnke, K.; Kern, K.; Kim, Y. Single-Molecule Phosphorescence and Intersystem Crossing in a Coupled Exciton Plasmon System. *ACS Nano* **2025**, *19*, 23796–23805.
29. Miwa, K.; Imada, H.; Imai-Imada, M.; Kimura, K.; Galperin, M.; Kim, Y. Many-Body State Description of Single-Molecule Electroluminescence Driven by a Scanning Tunneling Microscope. *Nano Letters* **2019**, *19*, 2803–2811.
30. Jiang, S.; Neuman, T. c. v.; Bretel, R.; Boeglin, A.; Scheurer, F.; Le Moal, E.; Schull, G. Many-Body Description of STM-Induced Fluorescence of Charged Molecules. *Phys. Rev. Lett.* **2023**, *130*, 126202.
31. Repp, J.; Meyer, G.; Paavilainen, S.; Olsson, F. E.; Persson, M. Scanning Tunneling Spectroscopy of Cl Vacancies in NaCl Films: Strong Electron-Phonon Coupling in Double-Barrier Tunneling Junctions. *Phys. Rev. Lett.* **2005**, *95*, 225503.
32. Fatayer, S.; Schuler, B.; Steurer, W.; Scivetti, I.; Repp, J.; Gross, L.; Persson, M.;

- Meyer, G. Reorganization Energy upon Charging a Single Molecule on an Insulator Measured by Atomic Force Microscopy. *Nat. Nanotechnol.* **2018**, *13*, 376–380.
33. Nazin, G. V.; Wu, S. W.; Ho, W. Tunneling rates in electron transport through double-barrier molecular junctions in a scanning tunneling microscope. *Proc. Natl. Acad. Sci. U.S.A.* **2005**, *102*, 8832–8837.
34. Kaiser, K.; Rosławska, A.; Romeo, M.; Scheurer, F.; Neuman, T. c. v.; Schull, G. Electrically Driven Cascaded Photon Emission in a Single Molecule. *Phys. Rev. X* **2025**, *15*, 021072.
35. Derry, G. N.; Kern, M. E.; Worth, E. H. Recommended values of clean metal surface work functions. *Journal of Vacuum Science and Technology A* **2015**, *33*, 060801.
36. Vasilev, K.; Doppagne, B.; Neuman, T.; Rosławska, A.; Bulou, H.; Boeglin, A.; Scheurer, F.; Schull, G. Internal Stark effect of single-molecule fluorescence. *Nature Communications* **2022**, *13*, 677.
37. Roy, P. P.; Kundu, S.; Makri, N.; Fleming, G. R. Interference between Franck–Condon and Herzberg–Teller Terms in the Condensed-Phase Molecular Spectra of Metal-Based Tetrapyrrole Derivatives. *The Journal of Physical Chemistry Letters* **2022**, *13*, 7413–7419.
38. Rukin, P.; Prezzi, D.; Rozzi, C. A. Excited-state normal-mode analysis: The case of porphyrins. *The Journal of Chemical Physics* **2023**, *159*, 244103.
39. Rukin, P. S.; Fortino, M.; Prezzi, D.; Rozzi, C. A. Complementing Adiabatic and Nonadiabatic Methods To Understand Internal Conversion Dynamics in Porphyrin Derivatives. *Journal of Chemical Theory and Computation* **2024**, *20*, 10759–10769.
40. Ferreira, R. C. d. C.; Sagwal, A.; Doležal, J.; Neuman, T.; Švec, M. Disentangling the

components of a multiconfigurational excited state in isolated chromophore with light-scanning-tunneling microscopy. *Nature Communications* **2025**, *16*, 6039.

41. Frisch, M. J.; Trucks, G. W.; Schlegel, H. B.; Scuseria, G. E.; Robb, M. A.; Cheeseman, J. R.; Scalmani, G.; Barone, V.; Petersson, G. A.; Nakatsuji, H.; Li, X.; Caricato, M.; Marenich, A. V.; Bloino, J.; Janesko, B. G.; Gomperts, R.; Mennucci, B.; Hratchian, H. P.; Ortiz, J. V.; Izmaylov, A. F. *et al.* Gaussian16 Revision C.01. 2016; Gaussian Inc. Wallingford CT.

Figures

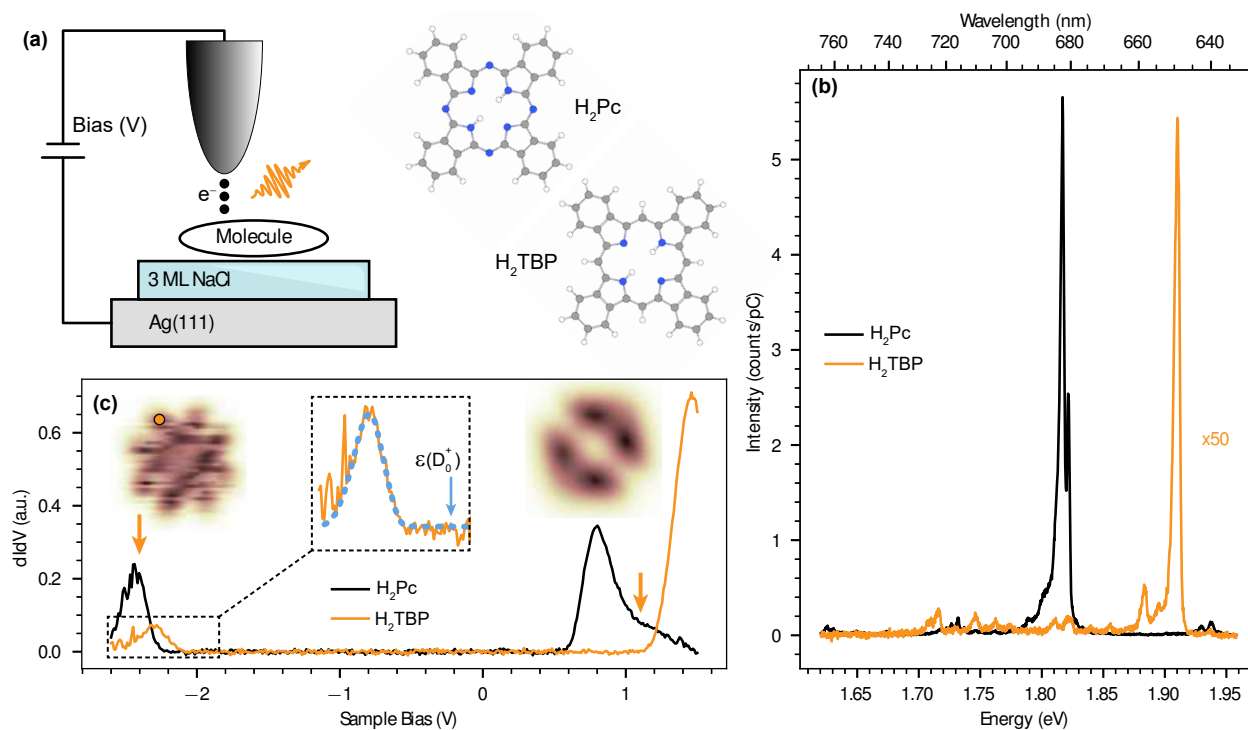


Figure 1: **Electronic and optical fingerprints of H₂TBP** (a) Cartoon of STM luminescence experiments of H₂Pc and H₂TBP adsorbed on a thin-film NaCl decoupling layer and supported by Ag(111). (b) Comparison of fluorescence intensity from single H₂TBP and H₂Pc molecules. STML of H₂TBP measured at -2.3 V and H₂Pc measured at -2.5 V. (c) Scanning tunneling spectroscopy of H₂TBP shown with comparison to H₂Pc to emphasize the upward shift of the molecular transport resonances. Constant-height STM images show the spatial distribution of the PIR and NIR recorded at -2.4 V and 1.1 V, respectively. The STS and STML data in panel b and c were recorded from molecules adsorbed on the same NaCl island with the same tip to ensure fair comparison of optical intensity. The inset in panel c shows a polaron model fit to the PIR, yielding a D₀⁺ state energy of 1.81 eV.

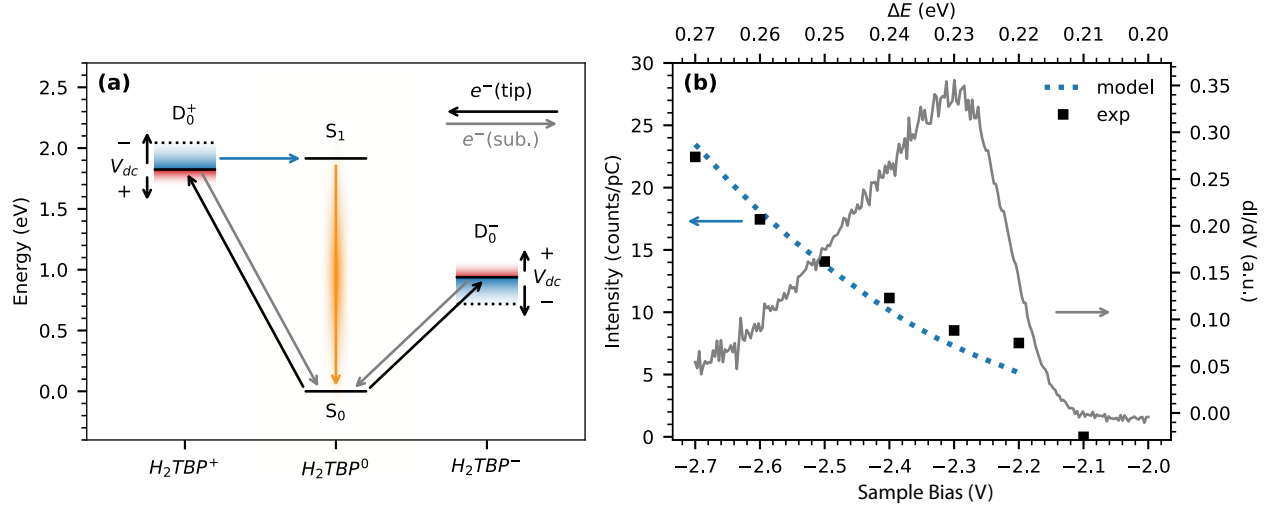


Figure 2: **Local tip gating in single molecule fluorescence** (a) Many-body diagram describing the electronic states of the H_2TBP molecule. Arrows connecting different H_2TBP charge states represent tunneling events while the orange arrow represents radiative relaxation (luminescence) from the first optical state. A shift in charge state chemical potential $\Delta E(V)$, due to the applied bias, is indicated by the shaded regions around the D_0^+ and D_0^- . Luminescence is detected when excitation and relaxation of the molecule follows the colored arrows from $D_0^+ \rightarrow S_1 \rightarrow S_0$. (b) [left axis] Bias dependent STML intensity of the 0-0 emission from S_1 of H_2TBP . Spectral intensity is integrated between 652 - 642 nm and normalized by the tunneling current and integration time. [right axis] STS spectra of the H_2TBP PIR. A rate equation model is used to simulate the voltage dependent emission rate (dashed blue line). The dashed lines in panel a represent the ΔE present at the onset of luminescence in panel b.

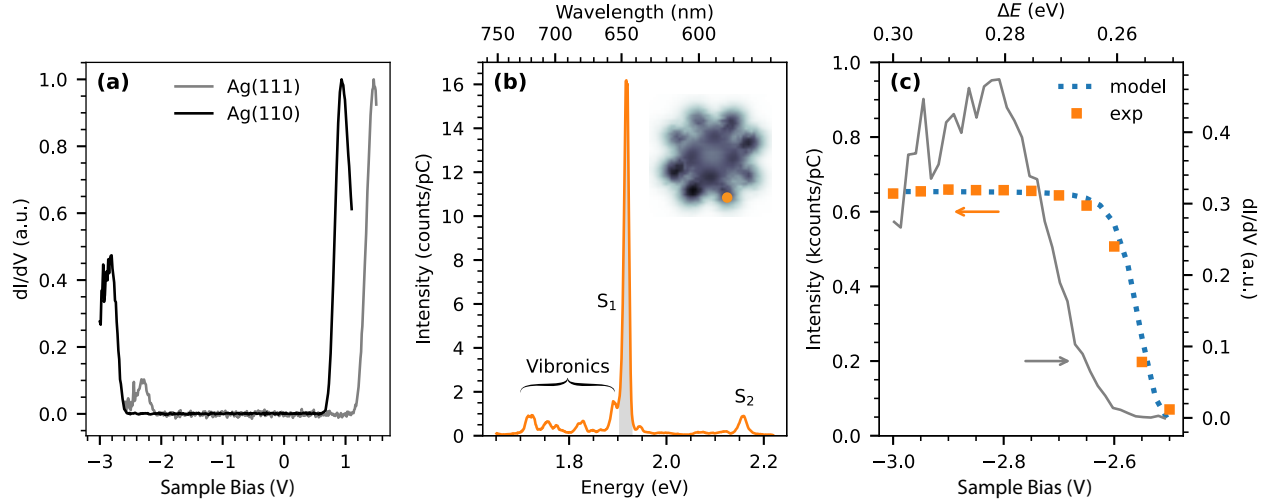


Figure 3: **Engineered energy level alignment for enhanced optical characterization** (a) Comparison of STS measurements of H_2TBP on Ag(111) and Ag(110). (b) STML spectra of H_2TBP adsorbed on NaCl/Ag(110). Measurement performed with $V = -3.0$ V, $I = -314$ pA and $t_{\text{acq}} = 15$ s. (c) [left axis] Bias dependent STML intensity of the 0-0 emission from H_2TBP . Spectral region is indicated by the grey shaded region in panel b and normalized by the tunneling current and integration time. [right axis] Reference STS spectra. Each of the measurements were recorded at the position indicated in the inset of panel b. The dashed blue line is represents the simulated voltage dependent emission rate, including a dark background current of 150 fA.

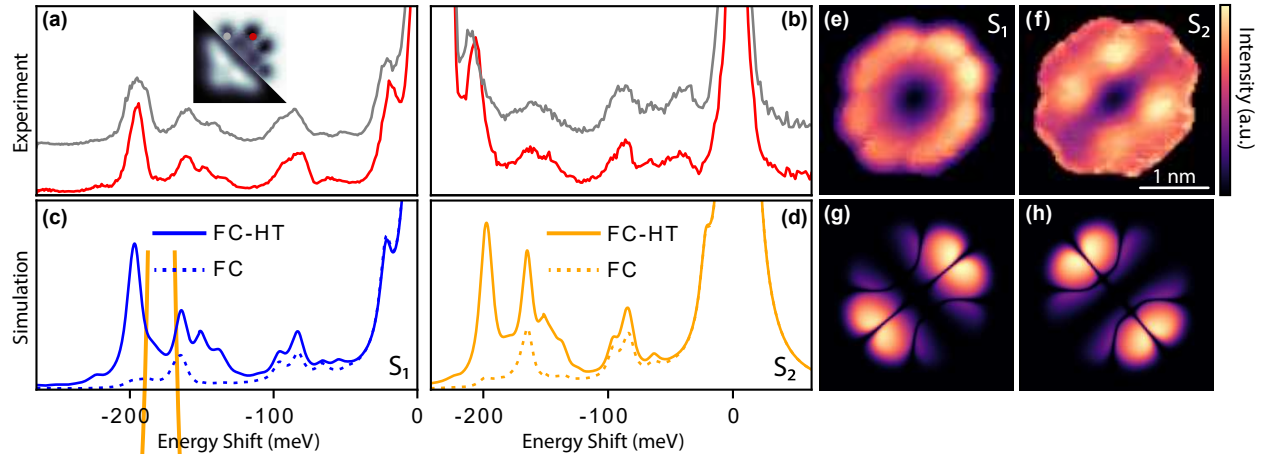


Figure 4: **High-resolution mapping and vibronic fingerprint of H_2TBP** (a) Vibronic emission from the S_1 zero-phonon-line at 1.91 eV. The STML spectra were measured with tip positions and molecule orientation indicated in the inset, using constant-height PIR and NIR images for reference. The spectra are vertically offset for clarity. (b) Vibronic emission from the S_2 zero-phonon-line at 2.15 eV. (c) and (d) TD-DFT calculation of Franck–Condon (FC) (dashed) and including Herzberg-Teller (FC-HT) (solid) assisted emission from gas phase geometry optimized for the S_1 and S_2 excited states. (e) and (f) STML intensity map of the S_1 and S_2 peak area. (g) and (h) Simulated STML map for the S_1 and S_2 states. The STML maps are recorded at -2.8 V and $t_{\text{acq}} = 15$ s.

Data availability

The data that support the findings of this study are available from the corresponding author upon request.

Acknowledgments

The authors would like to acknowledge Dr. Andres Ortega-Guerrero for his tremendous help educating us on DFT and TD-DFT calculations. His background in optical properties of porphyrin molecules was essential to our development of DFT calculation and analysis. We would also acknowledge fruitful discussions with Dr. Oliver Gröning and Prof. Roman Fasel. This research was funded by the Empa Young Scientist Fellowship and the European Research Council (ERC) under the European Union's Horizon 2020 research and innovation program (Grant agreement No. 948243). EA and NK appreciate financial support from the Werner Siemens Foundation (CarboQuant). For the purpose of Open Access, the author has applied a CC BY public copyright license to any Author Accepted Manuscript version arising from this submission.

Author contributions

EA and BS designed the experiments while measurements were performed by EA. NK was responsible for DFT/TD-DFT calculations, both EA and NK contributed to STML modeling, and all authors contributed to construction of the manuscript.

Competing interests

The authors declare no competing interests.

Supporting Information: Tunable Luminescence From a Single Free-Base Porphyrin Molecule By Controlled Access to Optically Active States

Eve Ammerman ^{1,*} Nils Krane ¹ and Bruno Schuler ¹

¹*nanotech@surfaces Laboratory, Empa – Swiss Federal Laboratories for Materials Science and Technology, Dübendorf 8600, Switzerland*

(Dated: January 26, 2026)

CONTENTS

Polaron Model	2
Rate Equation Model for Voltage Dependent Emission	3
Hyper-Resolved Fluorescence Maps	6
References	7

POLARON MODEL

The observed dI/dV peaks of molecules on NaCl are known to be, both, broadened and shifted to higher absolute energy, due to the strong electron-phonon coupling of the underlying salt [1, 2]. To extract the zero-phonon ion resonance energy, we employ a simple polaron model, as described by Vasilev et al. [3]:

$$S(E_{fi}, Q_{fi}, V) = \frac{1}{2\pi} \text{Re} \left\{ \int e^{-ieVt/\hbar} e^{\mathcal{F}(E_{fi}, Q_{fi})} dt \right\}, \quad \text{with} \quad (\text{S1})$$

$$\mathcal{F}(E_{fi}, Q_{fi}) = -iQ_{fi}E_{fi}t/\hbar + \int_0^\infty J(\Omega) e^{-iQ_{fi}\Omega t/\hbar} d\Omega, \quad (\text{S2})$$

where E_{fi} is the energy difference between final and initial state and Q_{fi} a unitless charge number, being +1 or -1 for hole or electron attachment, respectively. The electron-phonon coupling strength of the NaCl is included in the rectangular function $J(\Omega)$, which we assume to have a constant value η between $\Omega_{\min} = 18$ meV and $\Omega_{\max} = 31$ meV and is zero otherwise [3].

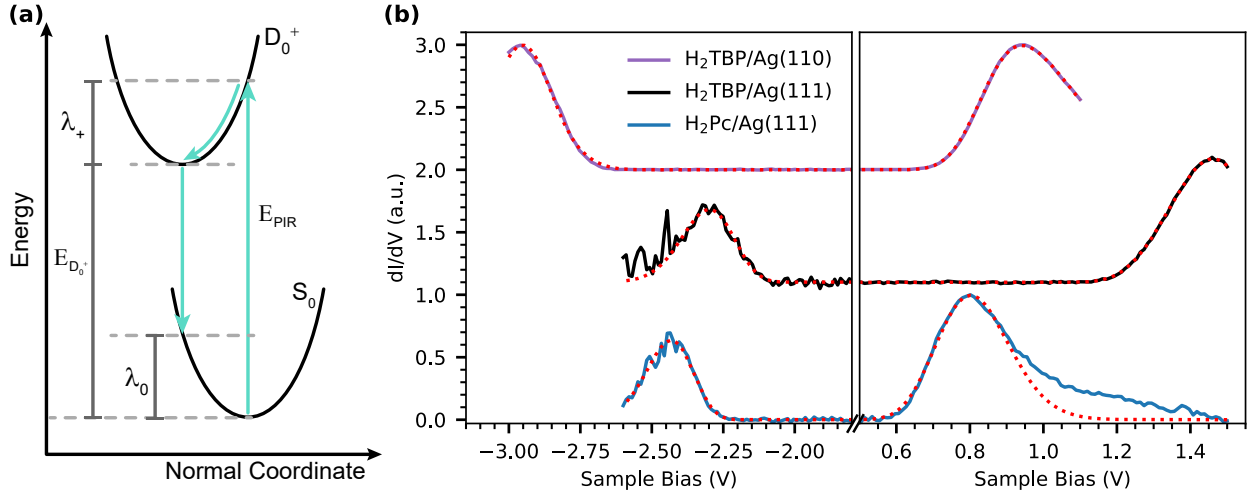


FIG. S1. **Polaron Modeling of dI/dV measurements.** (a) Sketch of the free-energy curves of a neutral and positively charged molecule on NaCl. The relaxation energy for ionization and neutralization are labeled λ_+ and λ_0 , respectively. (b) Experimental dI/dV spectra taken on TBP on Ag(110) (purple) and Ag(111) (brown) as well as Pc on Ag(111). Dotted red lines correspond to the model fit with respect to the corresponding dI/dV data.

The parameters E_{fi} and λ_{\pm} are used as fit parameters for the polaron model to the dI/dV spectra. Here, E_{fi} corresponds to the zero-phonon ion resonance energy (*cf.* E_{PIR} in figure

S1a) and λ_{\pm} is proportional to the electron-phonon coupling strength η :

$$\lambda = \int_0^{\infty} J(\Omega)\Omega \, d\Omega = \frac{\eta}{2} (\Omega_{\max}^2 - \Omega_{\min}^2) \quad (\text{S3})$$

Fitting was performed with a voltage scale of 0.9 to account for voltage drop across the NaCl. In Fig. S1 the x-axis of the fit data is rescaled to match the experimental data.

TABLE I. Fitted parameters obtained from polaron model.

Parameter	TBP/Ag(111)	TBP/Ag(110)	Pc/Ag(111)
$E_{D_0^+}$ (meV)	1812 ± 14	2248 ± 5	1984 ± 5
λ^+ (meV)	268 ± 11	303 ± 7	216 ± 6
$E_{D_0^-}$ (meV)	937 ± 8	544 ± 2	422 ± 6
λ^- (meV)	310 ± 11	297 ± 3	311 ± 7

RATE EQUATION MODEL FOR VOLTAGE DEPENDENT EMISSION

The voltage dependence of the emission rate was simulated with a simple rate equation model, similar to the one discussed in Ref. 4. Here we consider only three states (see Fig. 2a of the main text), namely S_0 , S_1 and D_0^+ . The energy $E_{S_1} = 1.915$ eV of the excitonic state is given by the experimentally measured photon energy of the 0-0 line and from the polaron fit, we extracted the the zero-phonon transition energy $E_{D_0^+}$.

The voltage dependent transition rates between the neutral and the charged state are given by integration of the polaron spectral profile as described in equation (S1):

$$\begin{aligned} \Gamma_{S_i \rightarrow D_0^+}^{t/s}(V_{\text{eff}}) &= \frac{2\hat{V}_{t/s}}{h} \int_{V_{\text{eff}}}^{\infty} S(E_{D_0^+} - E_{S_i}, +1, V') \, dV' \\ \Gamma_{D_0^+ \rightarrow S_i}^{t/s}(V_{\text{eff}}) &= \frac{\hat{V}_{t/s}}{h} \int_{-\infty}^{V_{\text{eff}}} S(E_{S_i} - E_{D_0^+}, -1, V') \, dV', \end{aligned}$$

with $\hat{V}_{t/s}$ being the coupling strength of the molecule to tip and surface. The effective bias voltage V_{eff} between molecule and corresponding lead is given by the voltage drop $\alpha \approx 0.1$ and corresponds to $V_{\text{eff}}^t = (1 - \alpha)V_b$ and $V_{\text{eff}}^s = -\alpha V_b$ for tip and sample, respectively. The additional factor of two for the singlet to doublet transition yields from multiplicities of the involved states and is given by the Clebsch-Gordan coefficients Υ_{fi} . As an approximation,

we assume the relaxation energy λ to be the same for all transitions between the positive ion resonance D_0^+ and the charge neutral states S_0 and S_1 ($\lambda_+^0 = \lambda_0^0 = \lambda_+^1 = \lambda_0^1$).

In the bias range of interest we further assume some transition rates to be constant, namely $\Gamma_{S_0 \rightarrow D_0^+}^s = \Gamma_{D_0^+ \rightarrow S_0}^t = \Gamma_{D_0^+ \rightarrow S_1}^t = 0$ as well as $\Gamma_{D_0^+ \rightarrow S_0}^s = \hat{V}_s/h$. We estimated the coupling to the substrate to be $\hat{V}_s = 4 \text{ meV}$ and used the coupling to the tip \hat{V}_t as a fitting parameter. For the radiative emission $\Gamma_{S_1 \rightarrow S_0}^{\text{opt}} = \hat{V}_{\text{opt}}/h$ the lifetime was estimated from the width of the emission peak to be in the order of $\hat{V}_{\text{opt}} = 1 \text{ meV}$.

In this simplified model we do not directly include the T_1 triplet state, since experimentally there is no indication of triplet pumping [4]. However, the presence of the triplet state causes an increase in the dark current as it opens another channel to neutralize the molecule via sample from the D_0^+ state into T_1 and then decay non-radiatively back into the ground state S_0 . To capture this effect, the transition rate $\Gamma_{D_0^+ \rightarrow S_0}^s$ is multiplied with a factor of 2.5, consisting of the Clebsh-Gordan coefficients $\Upsilon_{D_0^+ \rightarrow S_0} = 1$ and $\Upsilon_{D_0^+ \rightarrow T_1} = 1.5$.

The occupation probability N_i of the three considered states S_0 , S_1 and D_0^+ is solved using a differential rate equation for the steady state condition $0 = \sum_j \Gamma_{j \rightarrow i}(V_b)N_j - \Gamma_{i \rightarrow j}(V_b)N_i$ at given bias voltage V_b . The total current is then defined by $I_e(V) = e^-(\Gamma_{S_0 \rightarrow D_0^+}^t N_{S_0} - \Gamma_{S_1 \rightarrow D_0^+}^t N_{S_1})$ and the emitted light intensity by $I_{\text{opt}}(V) = A\Gamma_{S_1 \rightarrow S_0}^{\text{opt}} N_{S_1}$, with $A < 1$ representing the detection efficiency.

The modeled current and light intensity are fitted to experiment, using tip coupling \hat{V}_t , voltage drop α and photon detection efficiency A as fitting parameter. For the normalized STML intensity we added an additional background current $I_{\text{bg}} = 150 \text{ fA}$, corresponding to tunneling directly into the substrate: $I_{\text{opt}}/(I_e + I_{\text{bg}})$. The resulting fits are displayed in Fig. S2 and the corresponding parameter listed in table II. It is noteworthy, that the calculated STML intensity for H_2TBP on $\text{Ag}(111)$ is very sensitive to the voltage drop α , because the system is right at the onset regime of emission and slight changes in α cause an exponential increase or decrease in emission intensity. Accordingly, the obtained error value for α from the fit is only $4 \cdot 10^{-5}$ percent points. However, the value of α itself also depends on the estimated voltage drop used for the polaron fit, effectively increasing the actual error margin of α . Running the fit procedures for various voltage drop estimates showed that the best results were obtained for a voltage drop between 9 and 11% for $\text{TBP}/\text{Ag}(111)$.

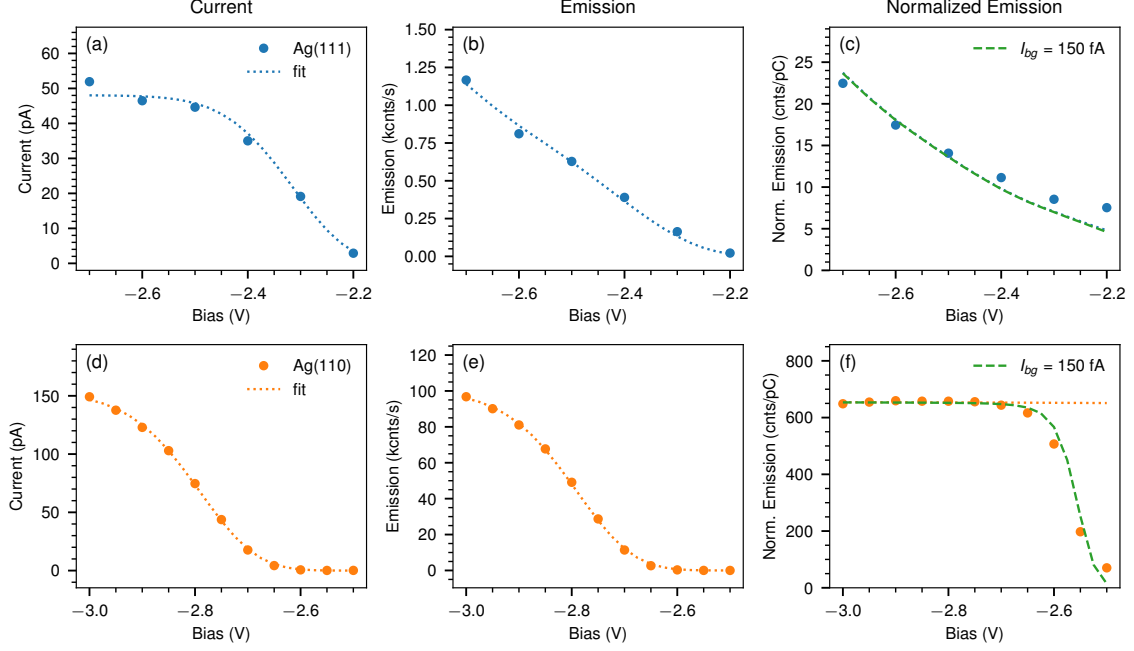


FIG. S2. **Modeling of STML data.** Bias dependent current and STML intensity of the 0-0 emission from H₂TBP on NaCl/Ag(111) (a-c) and NaCl/Ag(110) (d-f).

TABLE II. **Parameters used to model the STML intensity.** $E_{D_0^+}$ and λ^+ were obtained from the polaron model. A , α and \hat{V}_t were used as fitting parameters for the rate equation model.

Parameter	TBP/Ag(111)	TBP/Ag(110)
E_{S_0}		0 eV
E_{S_1}		1.915 eV
$E_{D_0^+}$	1.812 eV	2.248 eV
λ^+	268 meV	303 meV
A	$(1.27 \pm 0.05) \cdot 10^{-4}$	$(3.70 \pm 0.03) \cdot 10^{-4}$
α	10.2%	$(9.0 \pm 0.1)\%$
\hat{V}_t	$0.70 \pm 0.02 \mu\text{eV}$	$2.73 \pm 0.03 \mu\text{eV}$
\hat{V}_s		4 meV

HYPER-RESOLVED FLUORESCENCE MAPS

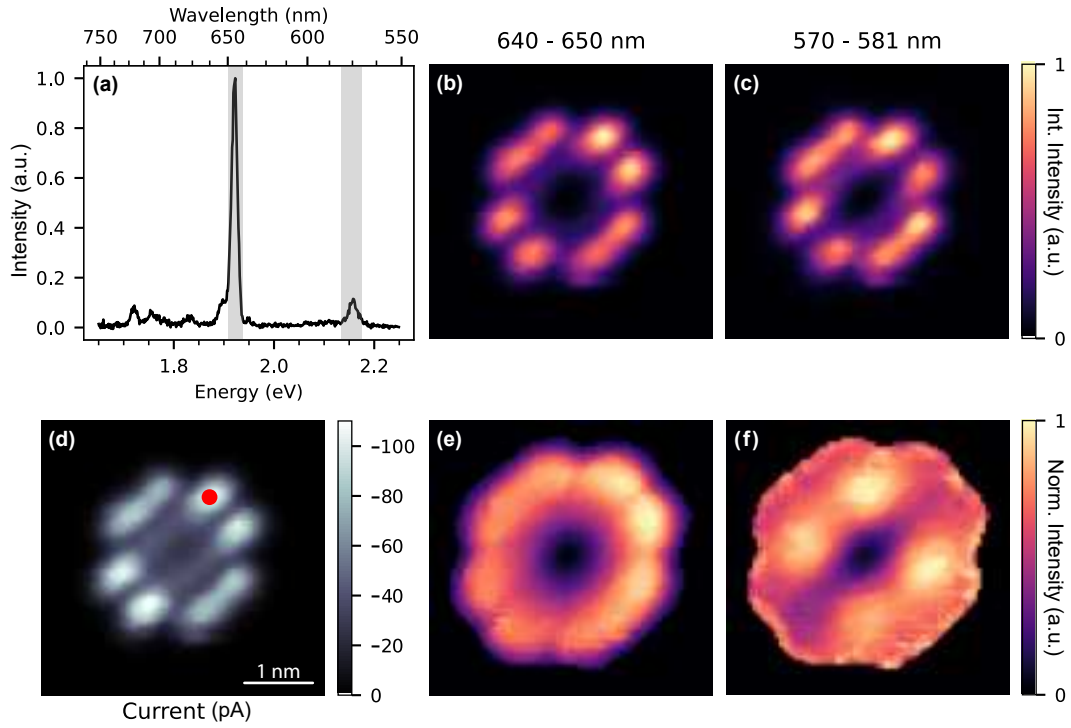


FIG. S3. **Hyper-resolved fluorescence maps of H_2TBP on 4-5 ML $\text{NaCl}/\text{Ag}(110)$** (a) Reference STML spectra recorded at the red dot indicated in panel d. Grey boxes mark the regions of integrated intensity for the maps shown in b and c. (b) and (c) Integrated intensity map of the S_1 and S_2 zero-phonon lines, respectively. (d) Average current recorded at each location during STML measurements. (e) and (f) Integrated intensity maps normalized by the current shown in panel d. To avoid division by zero, a background current of 1% of the maximum current was added to the tunneling current [5]. The maps are post-processed by a median filter to remove speckling originating from high amplitude cosmic ray peaks present in the individual spectra.

* eve.ammerman@empa.ch

- [1] J. Repp, G. Meyer, S. Paavilainen, F. E. Olsson, and M. Persson, [Phys. Rev. Lett. **95**, 225503 \(2005\)](#).
- [2] S. Fatayer, B. Schuler, W. Steurer, I. Scivetti, J. Repp, L. Gross, M. Persson, and G. Meyer, [Nat. Nanotechnol. **13**, 376 \(2018\)](#).
- [3] K. Vasilev, S. Canola, F. Scheurer, A. Boeglin, F. Lotthammer, F. Chérioux, T. Neuman, and G. Schull, [ACS Nano **18**, 28052 \(2024\)](#).
- [4] K. Kaiser, A. Rosławska, M. Romeo, F. Scheurer, T. c. v. Neuman, and G. Schull, [Phys. Rev. X **15**, 021072 \(2025\)](#).
- [5] A. Rosławska, T. Neuman, B. Doppagne, A. G. Borisov, M. Romeo, F. Scheurer, J. Aizpurua, and G. Schull, [Physical Review X **12**, 011012 \(2022\)](#).